Decay cascade of the $3d^{-1}$ vacancy in krypton clusters

Lutz Marder,[1,*] Catmarna Küstner-Wetekam,[1] Nils Kiefer,[1] Johannes Viehmann,[1] Niklas Golchert,[1] Emilia Heikura,[1] Florian Trinter,[2] Denis Cubaynes,[3] Jérôme Palaudoux,[4] Francis Penent,[4] Arno Ehresmann,[1] and Andreas Hans[1,†]

[1]*Institut für Physik und CINSaT, Universität Kassel, Heinrich-Plett-Straße 40, 34132 Kassel, Germany*

[2]*Molecular Physics, Fritz-Haber-Institut der Max-Planck-Gesellschaft, Faradayweg 4-6, 14195 Berlin, Germany*

[3]*Institut des Sciences Moléculaires d'Orsay, CNRS, Bâtiment 520, Université Paris-Saclay, 91405 Orsay-Cedex, France*

[4]*Laboratoire de Chimie Physique—Matière et Rayonnement, Sorbonne Université, CNRS, LCP-MR, 75005 Paris Cedex 05, France*

(Received 19 February 2026; accepted 29 September 2026; published 16 November 2026)

We report a comprehensive study of the decay cascade of $3d^{-1}$ vacancies of Kr atoms in clusters using coincident detection of up to four electrons and one ultraviolet photon. We find that the intra-atomic Auger decays predominantly proceed similarly to the atomic case, with a cluster counterpart identified for each major channel. Most Auger final states are of Kr^{2+} $4l^{-2}$ or $4l^{-3}$ nl' character, with $l = s$ or p and $l' = s$ or d. In strong contrast to the atomic monomers, where these final states decay radiatively to the ground state, in clusters all Auger final states decay via interatomic mechanisms, namely, different, sometimes exotic, variants of interatomic Coulombic decay, electron-transfer-mediated decay, and radiative charge transfer. Some pathways are enabled only once the clusters reach a minimum size, for example, when an energy transfer involves atoms beyond the first coordination shell. Competition between several interatomic channels and their cascading occurrence is observed. High-energy Auger final states undergo a second Auger step in atoms, leading to Kr^{3+} states, which is barely observed in clusters, likely due to interaction of Rydberg-like orbitals with neighboring atoms. Our study demonstrates the omnipresence, rich variety, and competition of interatomic processes in this prototype system following the absorption of a single x-ray photon.

DOI: 10.1103/9533-wm2s

I. INTRODUCTION

A. Photoionization of atoms

The spectroscopy of relaxation cascades following photoionization has been one of the main tools for the investigation of the electronic structure and photophysics of quantum systems for a long time. In isolated atoms, electronically excited states can in principle relax by two mechanisms: emission of an electron or a photon. For electronic vacancies in inner shells with not too high binding energies, autoionization—Auger decay—is typically the dominant process. Photon emission takes over for states with low binding energies in which electron emission is energetically not possible, or for deep holes of heavy elements, where x-ray emission is favored.

Depending on the shell of the initial electronic vacancy, Auger electron emission can proceed in a single step or in a cascade of several steps [1–5]. Electron correlations, moreover, may enable the simultaneous emission of more than one Auger electron in double or triple Auger decays [3,4]. Consequently, for a given initial state, a probability distribution for decays into the quantum-mechanically allowed final ionic states can be determined, which is characteristic for the particular electronic system and intra-atomic interactions.

B. Interatomic decay channels

Over the last few decades, it has been predicted theoretically and demonstrated experimentally in numerous systems and scenarios that new relaxation channels open once an atom is placed in an environment, e.g., within a cluster. This remains true even if the bonds are so weak that the electronic structure of the atom can still be assumed to be atomiclike [6]. In these weakly bound systems, neighboring atoms have been found to take part in the decay as the multiple ionization potentials of the extended system are energetically lower than those of an isolated atom.

In interatomic Coulombic decay (ICD), an electronically excited atom relaxes and transfers the excess energy to a neighboring atom, whereby the latter is ionized [6–8]. If orbital overlap is small, ICD is typically described as the transfer of a virtual photon between the atoms [9]. Consequently, in the atomic picture, this conventional or "direct" ICD must obey the dipole selection rules [10]. In a larger cluster, however, due to symmetry breaking the selection rules are softened [11]. For atoms closer to each other, "exchange" ICD may contribute, which is mediated by the transfer of an electron from a neutral neighbor and therefore relies on orbital overlap, which scales exponentially with the internuclear distance [12]. That way, the initially excited (ionized) atom receives an electron but becomes ionized by the excess energy and finally remains in its charge state.

*Contact author: lutz.marder@uni-kassel.de

†Contact author: hans@physik.uni-kassel.de

Published by the American Physical Society under the terms of the Creative Commons Attribution 4.0 International license. Further distribution of this work must maintain attribution to the author(s) and the published article's title, journal citation, and DOI.

Electron-transfer-mediated decay (ETMD) is a related process in which an electron from a neutral neighbor is transferred to an electronic vacancy and another electron is emitted [13,14]. In contrast to exchange ICD, the emitted electron originates from the donating atom [ETMD(2)] or from a third site [ETMD(3)]. Recently, ETMD(4) has been observed experimentally, in which two electrons from two neutral neighbors are transferred at the same time, (partially) neutralizing the charge of a highly charged ion, and a fourth site is ionized [15]. Finally, charge transfer can also proceed radiatively via radiative charge transfer (RCT) [16] if the excess energy gained from charge delocalization is not enough for further ionization of the whole system, resulting in the emission of a photon. RCT is, like ICD and ETMD, a purely environmental phenomenon. Evidently, interatomic processes significantly alter the final charge distribution and state of a system after its decays. The total charge state can be increased through one or a cascade of several ICD and/or ETMD processes, while mainly ETMD and RCT lead to charge delocalization.

So far, many different variants of ICD, ETMD, RCT, and related processes have been extensively discussed in the literature, most of them both theoretically and experimentally [6]. In the present work, we provide a comprehensive study of the full relaxation cascades of a prototypical $3d$ inner-shell vacancy of Kr atoms in clusters. After photoionization of the $3d$ electron, the initial states are populated through Auger decays of the $3d^{-1}$ vacancy into states of Kr^{2+} $4l^{-2}$ or $4l^{-3}\,nl'$ electron configurations, with $l = s$ or p and $l' = s$ or d. The interatomic decay of Auger final states in Kr has been observed before [17]; however, the study in Ref. [17] was performed on *dimers* as target systems, which offers the possibility of applying momentum spectroscopy of the resulting ions. We demonstrate that the decay cascade changes drastically for larger clusters as a result of the availability of more and more distant neighbors. Our study provides the first state-selective overview over the full decay cascade enabled by a powerful multicoincidence technique in which multiple electrons are detected together with photons.

If many neighbors are available, *all* Auger final states decay through interatomic channels, and, in general, a rich variety of different ICD, ETMD, and RCT processes is triggered by a single soft x-ray ionization. Our study strikingly underlines the universality of interatomic processes and their omnipresence and diversity.

The article is organized as follows. Section II describes the experimental method. The $3d$ Auger spectra of Kr atoms in clusters compared to the ones of monomers and the population distribution of the different Auger final states, which at the same time are the initial states of interatomic processes, are presented in Sec. III. In Sec. IV, each Auger final state and the resulting cascade is discussed individually.

II. EXPERIMENT

The results presented here have been recorded in two different experiments using different but in principle similar setups, which are described in the following. In both cases, electron-photon multicoincidence experiments were conducted on clusters, combining a cluster source with a magnetic-bottle-type electron spectrometer (MBES) and a photon detector.

Before each measurement, the event rate was carefully adjusted to reduce the probability of random coincidences, where particles originating from different photoionization events are falsely attributed to the same event. A statistical evaluation involving pairs of adjacent time windows, each containing a single excitation event, was used to confirm the insignificance of these random events.

A. Kr $3d$ Auger measurements

The data discussed in Sec. III, containing the Auger decay following Kr $3d$ ionization, were measured at the UE56-2_PGM-2 beamline [18] located at the BESSY II storage ring of Helmholtz-Zentrum Berlin. The customized setup was built specifically for the investigation of electron emissions from rare-gas clusters with an MBES [19,20] together with photon detection by a single-photon detector [21]. The unique coincident photon-electron detection scheme used in the present work enables the efficient elimination of the electron signal from monomers, which is always present in experiments with mixed cluster beams. Here, the fact is used that the recorded photons can only be emitted by the cluster-specific RCT process, which is absent in monomers [22].

As photon-electron coincidence measurements have historically been scarce due to the large disparity between the solid angles for electron and photon detection, a dedicated mirror assembly has been integrated into the setup, substantially increasing the solid angle for photon detection [21]. This combination enables the coincident detection even of multiple electrons with photons, in the present configuration in the ultraviolet (UV) range of approximately 4–10 eV, which is the relevant spectral range for the expected photon emission in Kr clusters from RCT processes [15]. The sensitivity range for the MCP-based single-photon detector is specified by the CsTe photocathode coated on a MgF_2 entrance window [23] and events are recorded by a hexagonal delay-line anode. The MBES is based on an established design [2,20], adapted to the temporal spacing between successive synchrotron light pulses in the single-bunch mode at the BESSY II storage ring of about 800 ns with a 60 cm drift tube and an entrance aperture without meshes. To increase the absolute resolution of the recorded electron energies, a retardation potential can be applied to the drift tube, and a combination of a permanent magnet with a soft-iron truncated-cone tip and a solenoid produces a bottle-shaped magnetic field that effectively collects and guides the ejected electrons toward the MCP-based detector [24]. The resolving power of the instrument was determined to be approximately $E/\Delta E = 30$ in earlier experiments under comparable conditions [20] and is assumed to be similar here.

The Kr clusters are produced in an expansion chamber adjacent to the interaction chamber, separated by a conical 1 mm skimmer to cut off large parts of the monomer gas surrounding the cluster jet. However, a significant amount of noncondensed target remains within the jet, meaning that all spectra inherently originate from a target composed of both free atoms and clusters. The cluster source is cryogenically cooled by a liquid-nitrogen cryostat set to $T = 130\,\mathrm{K}$ and a

stagnation pressure of $p = 550$ mbar is maintained by a steady flow of 14 sccm Kr gas through a conical nozzle of 80 μm diameter and 30° full-opening angle. According to conventional scaling laws [25,26], this results in a mean cluster size of $\langle N \rangle \approx 190$ atoms per cluster. Note that clusters produced by supersonic expansion exhibit a wide distribution of sizes around the estimated mean value, which leads to a broadening of the electronic features [27].

The Kr $3d$ Auger spectra presented in this article (see Sec. III) are a result of five individual measurements with different exciting-photon energies (97.0, 107.5, 117.5, 127.5, and 137.5 eV) and voltages (+3 V acceleration, −10, −20, −30, and −39 V deceleration, respectively) that have been combined into a continuous spectrum. Thus, a good experimental resolution can be ensured throughout the detected electron kinetic-energy range of up to 66 eV.

B. Auger final-state decay measurements

The central results, concerning the intra- and interatomic decay of doubly charged Kr states presented in Sec. IV, have been extracted from measurements recorded at the soft x-ray spectroscopy beamline PLEIADES at Synchrotron SOLEIL using an exciting-photon energy of 150 eV. This yields $3d$ photoelectrons with kinetic energies between 54 and 58 eV, which includes both fine-structure components $3d_{3/2}$ and $3d_{5/2}$ from atomic and cluster sites, broadened by cluster-typical effects (see above) and the limited resolution of the electron spectrometer. The synchrotron light pulses are generated by an APPLE-II permanent-magnet undulator (HU 80) and are monochromatized by a plane grating monochromator; their temporal spacing in the single-bunch operation mode is 1181 ns.

The setup used for these experiments uses a similar principle, but a different variant of the MBES. The HERMES spectrometer provides a longer drift tube with a length of 2.4 m, increasing the energy resolution to around $E/\Delta E = 60$ while maintaining a high detection efficiency of about 50%, as deduced from earlier experiments [2,4,28]. The collection mirror assembly was adapted to match the differing geometry of the experiment, further increasing the photon yield; the photon detector used was identical to that described above.

In this experiment, the Kr clusters were produced using a smaller nozzle of 60 μm diameter (30° full-opening angle) and a stagnation pressure of around 2.5 bar at room temperature, which yields an estimated mean cluster size of $\langle N \rangle \approx 60$ atoms per cluster [25]. A skimmer of 0.3 mm diameter was used to reduce the amount of noncondensed atoms in the cluster jet. To collect all emitted electrons, especially the very slow ones that are of particular interest in this study, within the period between two consecutive light pulses, an accelerating voltage of +13 V was applied to a mesh at the entrance of the MBES and to the drift tube.

III. KR $3d$ AUGER DECAY IN CLUSTERS

For the present study, the decay of the $3d^{-1}$ vacancy was chosen, which is well investigated in the atomic case and known to be dominated by Auger decays, yielding an involved electron spectrum [28,29], eventually with subsequent photon emission if the final state of the Auger decay is not the ionic ground state [30]. The Auger electron spectrum extends to about 55 eV for the channels with the highest kinetic energies. These kinetic energies are still small enough for a coincident detection of an Auger electron and a slow electron from an interatomic process with decent energy resolution when the atom is embedded in a cluster.

The Kr $3d^{-1}$ Auger spectrum can be divided into two main regions. In the kinetic-energy range above approximately 20 eV, the remaining binding energies of the single-step Auger final states are not sufficient for a second Auger step in atoms, and therefore, the Auger decay either leads directly into the Kr^{2+} ionic ground state or the ground state is reached by subsequent fluorescence [30]. The Kr^{2+} Auger final states are of two-hole or three-hole–one-particle character with all holes in the N shell, which can be written as Kr^{2+} $4l^{-2}$ or $4l^{-3}\,nl'$, with $l = s$ or p and $l' = s$ or d [28]. If the first Auger electron has less than 20 eV kinetic energy, a second Auger step is possible with the emission of another electron, possessing a kinetic energy of under 10 eV [28,29]. For such low kinetic energies, the disentanglement of local Auger decay and interatomic processes becomes difficult, which is why we will first focus on the range of Auger electron kinetic energies above 20 eV and discuss the lower-kinetic-energy range later.

The measured Kr $3d^{-1}$ Auger spectrum above 15 eV is shown in Fig. 1. Using coincident detection with a $3d$ photoelectron, the total spectrum has been disentangled into contributions from the two fine-structure components $3d_{3/2}^{-1}$ and $3d_{5/2}^{-1}$ as well as into contributions from atoms and clusters. The atomic spectra agree reasonably well with the spectra from the literature and exhibit a characteristic difference of about 1.2 eV between the kinetic energies of electrons emitted from the two $3d$ fine-structure components, corresponding to the spin-orbit splitting.

For each of the most prominently populated Auger final states, a cluster equivalent can be identified. In the clusters, all Auger electron energies are shifted toward higher kinetic energies compared to the atomic counterparts. The magnitudes of this shift $\Delta E_{\mathrm{kin}}^{\mathrm{a\text{-}c}}$ are listed in Table I and range from 2.1 to 2.8 eV. These differences are well known for cluster spectra and originate from polarization screening due to the environment [27,31,32]. Moreover, the cluster features are also broadened, which can mainly be attributed to the distribution of different cluster sizes in the target (see Sec. II). In the spectra, six main features are discernible (see Fig. 1). Due to the broadening, some channels of relatively weak intensity, visible in the atomic spectra, cannot be unambiguously identified in the cluster spectra and will, therefore, not be discussed further. The kinetic energies of the Auger electrons and binding energies of the Auger final states for the main channels as observed in the present experiment (positions of maxima in Fig. 1) are listed in Table I and assigned to the dominant electronic configuration by comparison with the atomic case, where the configurations are known from the literature [28,33].

TABLE I. The most prominent Kr $M_{4,5}NN$ Auger final states as observed in Fig. 1. The respective Auger electron kinetic energies E_{kin} are taken directly from the spectra for each fine-structure component for both atoms and clusters. Final-state binding energies E_{B} are relative to the ground state of the neutral atom; for clusters, they have been calculated by taking the exciting-photon energy and energies of the coincidentally detected electrons (photoelectron and Auger electron) into account. In the last column, the energy differences between Auger electron kinetic energies in atoms and clusters $\Delta E_{\mathrm{kin}}^{\mathrm{a\text{-}c}}$ are shown. See main text for more details. All energies are given in eV.

	Atom			Cluster			
	E_{kin}			E_{kin}			
Auger final state	$3d_{3/2}^{-1}$	$3d_{5/2}^{-1}$	E_{B}	$3d_{3/2}^{-1}$	$3d_{5/2}^{-1}$	E_{B}	$\Delta E_{\mathrm{kin}}^{\mathrm{a\text{-}c}}$
$4p^{-2}\,{}^3\mathrm{P}$	56.4	55.2	38.4	59.2	58.1	34.6	2.8
$4s^{-1}\,4p^{-1}\,{}^3\mathrm{P}$	42.4	41.1	52.7	44.5	43.1	49.6	2.1
$4p^{-3}\,4d\,{}^5\mathrm{D}$	39.2	37.9	55.5	41.4	40.2	52.6	2.2
$4p^{-3}\,4d\,{}^3\mathrm{P}$	32.3	31.0	61.8	34.7	33.4	59.2	2.4
$4s^{-2}$	25.1	23.9	69.6	27.5	26.2	66.3	2.4
$4s^{-1}\,4p^{-2}\,5s$	16.8	15.4	77.9	19.3	17.9	74.8	2.5

IV. DECAY OF AUGER FINAL STATES

A. Overview

Figure 2(a) shows a two-dimensional map of events where three electrons have been coincidentally detected, namely, the $3d$ photoelectron, the Auger electron, and a third electron. These events are plotted as functions of the Auger final-state binding energy (obtained through the photoelectron and Auger electron kinetic energies) on the horizontal axis and the kinetic energy of the third emitted electron on the vertical

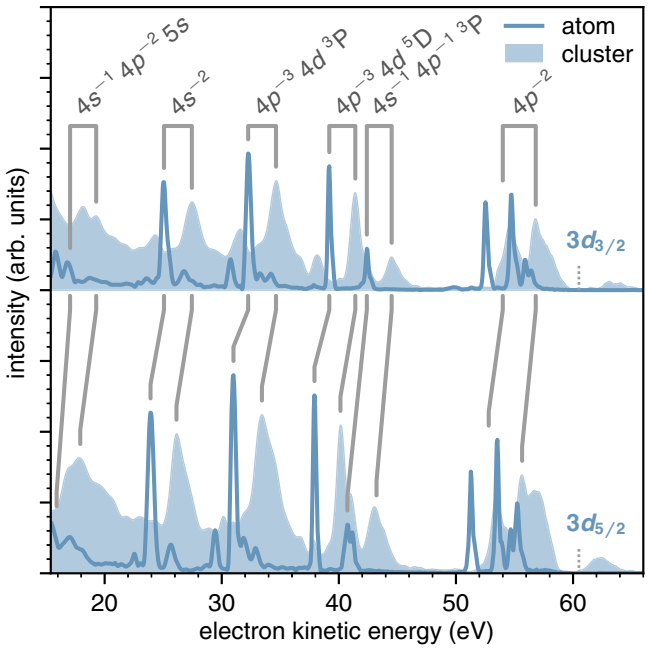


FIG. 1. The Kr $M_{4,5}NN$ Auger spectra recorded in coincidence with photoelectrons emitted from the $3d_{3/2}$ (upper panel) and $3d_{5/2}$ (lower panel) orbitals, starting at around 15 eV Auger electron kinetic energy for both atoms (solid line) and clusters (filled area). The full spectrum is merged from five individual measurements with different experimental parameters to achieve a decent energy resolution throughout the whole spectral range. The six most prominent features can be clearly distinguished and are identified using literature assignments on the atomic case [28], with the respective cluster feature broadened and shifted toward higher kinetic energies. For each feature, the relevant energies are listed in Table I. The relatively weak features at highest kinetic energies originate from core-level ICD and are upscaled by a factor of 5.

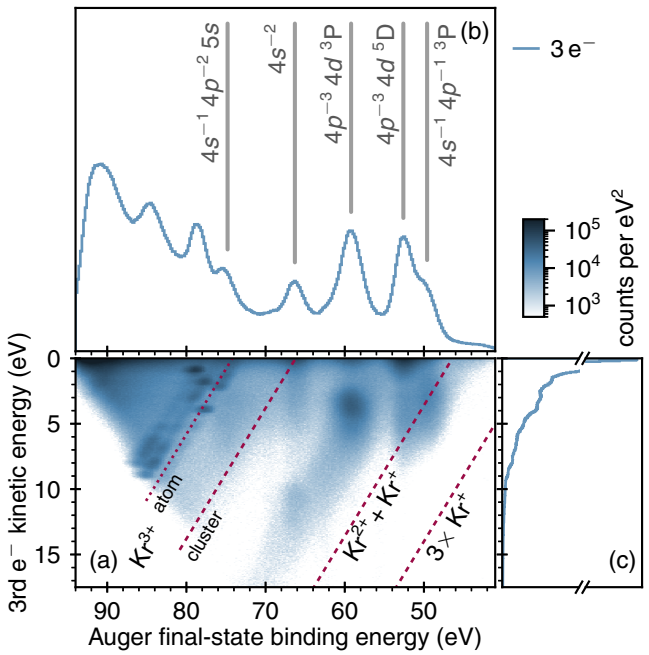


FIG. 2. Three-electron coincidence map (a) showing triple coincidences as functions of the Auger final-state binding energy (obtained through the kinetic energies of the coincidentally detected photoelectrons and Auger electrons) and the kinetic energy of the third detected electron. (b) Photoelectron–Auger electron coincidence spectrum, obtained by integrating over the full energy range of the third detected electron. (c) Emission probability distribution of the third electron, coincidentally detected with the photoelectron and the Auger electron, as a function of its kinetic energy and obtained by integrating all Auger final states. Diagonal lines in the map (a) indicate limits below which the respective ion configuration cannot be reached energetically. Each observed feature in the map corresponds to one or more transitions that belong to decay processes of the doubly charged states.

axis. Panels (b) and (c) of Fig. 2 show projections of the map onto the respective axis, i.e., the integrated spectra of the Auger final-state binding energy and the third electron kinetic energy, respectively. The region of the Kr^{2+} $4p^{-2}$ Auger final state is excluded from the map, since it overlaps with the $3d$ photoelectron at the present conditions (see Sec. II) and cannot lead to further electron emission (see Sec. IV B). All other Auger transitions to states above 50 eV binding energy are followed by successive emissions of further electrons in clusters. The respective spectra of the emitted third and a possible fourth electron will be evaluated in separate sections below. Note that the map and spectra in Fig. 2 are empty for Kr monomers for binding energies below the atomic Kr^{3+} threshold, since none of the Auger final states in that spectral range possesses a binding energy high enough for further ionization. This threshold is shown in Fig. 2 as a dotted diagonal line. Although the cluster one-site triple-ionization potential—indicated by a dashed diagonal line—is shifted considerably compared to the atomic case, it is still beyond most of the Auger final states (just reaching the $4s^{-2}$ state). In stark contrast to that, the ionization thresholds with charges delocalized in $Kr^{2+} + Kr^{+}$ or $3\times Kr^{+}$ lie much lower and are accessible. Their positions have been estimated using the shifts of the Kr $4p$ and $3d$ ionization thresholds in the cluster bulk as reported by Feifel *et al.* [27].

The correlation map between the populated Auger final state and the third measured electron under the additional condition that also a photon is detected in coincidence (i.e., $3\,e^- + h\nu$) is shown in Fig. 3(a) and the projections of the spectra in Figs. 3(b) and 3(c), respectively. The spectrum from $3\,e^-$ coincidences [as shown in Fig. 2(b)] is also plotted in Fig. 3(b) for comparison. Features in Fig. 3(a) represent a subset of the features of Fig. 2(a).

The diagonal lines in the correlation maps [e.g., Figs. 2(a) and 3(a)] for the delocalized charge states represent the potential energies at infinite distances between the ions. In general, and, in particular, for the ionization of a cluster, the sum of the pairwise Coulomb energy between the ions according to

$$E_C(R_{i,j}) = \sum_{i \neq j} \frac{1}{4\pi\varepsilon_0} \frac{q_i q_j}{R_{i,j}} \tag{1}$$

must be considered. Note that this model allows for an estimate of the Coulomb energy between ground-state ions only, neglecting screening effects or shifts due to possibly populated excited orbitals. In Fig. 4, we present an overview of potential energy curves (PECs), each representing the potential energy as a function of the internuclear distance for the relevant final states of interatomic processes (the choice of states will become more evident below).

The asymptotic values of the PECs at large distances are given by the sum of the binding energies of the populated ionic states. In all cases, at least one Kr^{+} $4p^{-1}$ ion is present, the binding energy of which relative to the neutral ground state corresponds to the single-ionization potential of Kr clusters. Its value of 12.0 eV is taken from the literature [27]. For the ionic $4p^{-2}$ configuration, the three fine-structure components ^{3}P, ^{1}D, and ^{1}S are shown, with the latter two assumed to lie 1.7 and 4.0 eV above the ^{3}P ground state, respectively, as is the case for atoms. Binding energies for the other states are

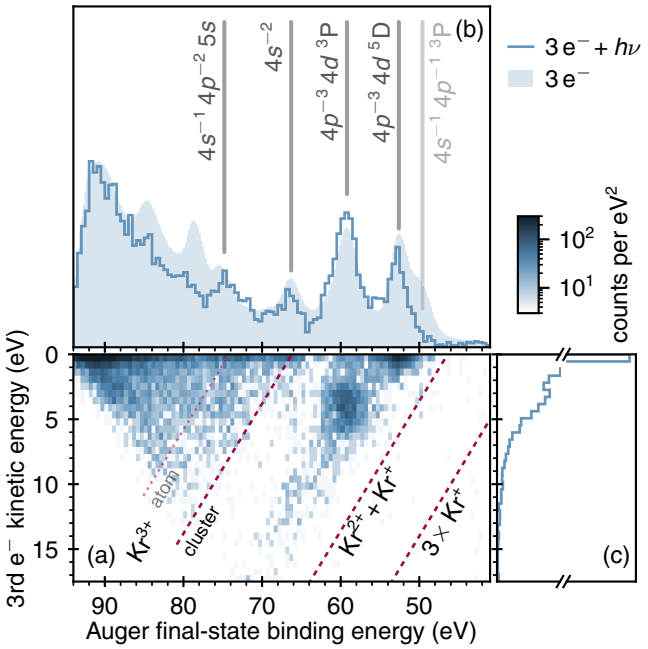


FIG. 3. Three-electron–one-photon coincidence map (a) showing quadruple coincidences as functions of the Auger final-state binding energy (obtained through the kinetic energies of the coincidentally detected photoelectrons and Auger electrons) and the kinetic energy of the third detected electron. (b) Photoelectron–Auger electron coincidence spectrum, obtained by integrating over the full energy range of the third detected electron. (c) Emission probability distribution of the third electron, coincidentally detected with the photoelectron and the Auger electron and a UV photon, as a function of its kinetic energy and obtained by integrating all Auger final states. The three-electron spectrum without coincident photon detection from Fig. 2 is depicted as a shaded area in panel (b).

estimated as discussed below. It should be noted that the values used represent an energy shift corresponding to atoms within the bulk of the cluster. Atoms at the surface may have slightly higher binding energies, and for samples with different mean cluster sizes, the contributions from bulk and surface atoms will differ. The present data do not allow for separation of surface and bulk contributions. However, due to the widths of the states, it is expected that most of the discussed transitions can also occur involving surface atoms, and the bulk values are used without loss of generality.

The indicated equilibrium distance R_{eq} is that of a neutral Kr dimer, 4.02 Å [34], which has also been used in the calculations. Although this distance may slightly decrease in larger clusters, this effect should be negligible for the following discussion.

For states with three ions, two PECs are shown, for the Coulomb energy calculated in a linear and a triangular geometry (see figure caption). On the right side of the diagram, the Auger spectrum leading to triple ionization is shown. Horizontal dotted lines indicate the potential energy of the respective Kr^{2+} Auger final state. From the relative positions of these states and states with a total of three—now delocalized—charges, it can be estimated which of the interatomic decay processes may be operable; in the following, this will be discussed in detail for each state individually.

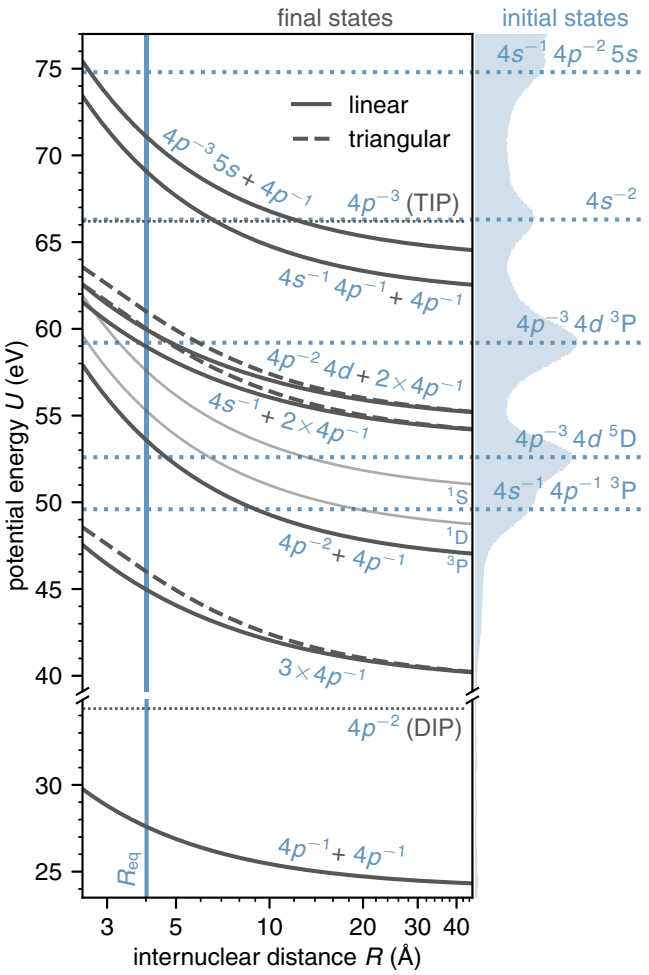


FIG. 4. Potential energy curves for relevant final states that can be reached by relaxation of the doubly charged initial states, depicted as the potential energy as a function of the internuclear distance. The initial states are populated by a preceding Kr $M_{4,5}NN$ Auger decay, whose spectrum is shown as a shaded area to the right, and their binding energies are indicated as dotted blue horizontal lines. The Kr cluster double (DIP) and triple (TIP) ionization potentials are also shown. A blue vertical line shows the equilibrium distance R_{eq} of a neutral Kr dimer of 4.02 Å [34]. For those final states containing three ions, PECs are also given for a triangular (T shape, with a dimer static at equilibrium and the third site perpendicular at varying distance; dashed lines) in addition to the linear geometry. Transitions are possible only into final states whose PECs lie energetically below the initial-state potential energy. For some states, the channels only open at a specific internuclear distance, possibly larger than the equilibrium distance R_{eq}.

B. Auger final state $4p^{-2}$

The Auger channel emitting electrons with highest kinetic energy leads into the Kr^{2+} $4p^{-2}$ $^3P_2$ dicationic ground state with 34.4 eV binding energy in the cluster. The other triplet states $^3P_{1,0}$ are only separated by about 0.3 eV and cannot be resolved in the cluster spectrum. The ^{1}D and ^{1}S states of the $4p^{-2}$ electron configuration cannot undergo any further (local or nonlocal) autoionization since their maximum excess energy with respect to the ionic ground state lies below 4 eV. However, in clusters, all these states can decay by RCT: A valence electron from a neutral neighboring atom fills one of the two $4p$ vacancies and the energy gained by the charge delocalization is emitted as a photon in the UV spectral range. On the high-kinetic-energy side of the $4p^{-2}$ Auger channels in Fig. 1, a weak feature (depicted upscaled by a factor of 5 for better visibility) can be identified with a few eV separation. This feature indicates the direct ICD of the inner-shell vacancy (so-called core-level ICD). In the present coincidence data, the Kr^{2+} $4p^{-2}$ channel cannot be isolated as it overlaps in kinetic energy with the $3d$ photoelectrons (see Sec. II). However, both RCT [22] and core-level ICD [35] have already been discussed in detail elsewhere and are not the focus of this study.

C. Auger final state $4s^{-1}4p^{-1}$ ^{3}P

The feature in the Auger electron spectrum with the second highest kinetic energy corresponds to a dicationic electron configuration with one vacancy in each of the $4p$ and $4s$ valence orbitals, Kr^{2+} $4s^{-1}4p^{-1}$ ^{3}P. The state has a potential energy of 15.2 eV with respect to the dicationic ground state, i.e., a total binding energy of 49.6 eV. The corresponding emission spectra for three-, four-, and five-particle emission (i.e., $3\,e^-$, $3\,e^- + h\nu$, $4\,e^-$, and $4\,e^- + h\nu$) are shown in Fig. 5(a) combined with an enlarged view of the PEC diagram with the region of interest for this particular state in Fig. 5(b). All spectra are filtered for only those electrons that are correlated with the $3d$ photoelectron and the Auger electron leading to the $4s^{-1}4p^{-1}$ ^{3}P state.

The $3\,e^-$ spectrum shows two prominent features: the first (labeled I) peaks toward 0 eV kinetic energy and extends up to about 2 eV, and the second (labeled II) covers the relatively broad range from 0 eV to about 7 eV, peaking around 3 eV. Although both features overlap and their relative contributions can therefore not be quantified precisely, it seems evident that feature II exhibits a significantly higher total intensity than feature I. In the spectra with four or five coincident particles, the only feature discernible from the noise is the emission of three electrons and one photon at feature I.

A seemingly straightforward interatomic decay path for the $4s^{-1}4p^{-1}$ ^{3}P state is ICD with a $4p$ electron relaxing into the $4s$ vacancy and leading to the emission of another $4p$ electron from a neighboring atom. As a final state, only the ^{3}P component is reasonable due to the selection rules regarding spin conservation. However, considering the PEC diagram, we find that the PEC of the ICD final state $Kr^{2+}(4p^{-2}$ $^3P) + Kr^+(4p^{-1})$ intersects the Kr^{2+} $(4s^{-1}4p^{-1})$ initial-state energy only at an internuclear distance of about 9 Å, which is slightly more than twice the equilibrium internuclear distance of a neutral Kr dimer $R_{eq} = 4.02$ Å [34]. Consequently, no direct neighbors can be ionized by the ICD process due to the Coulomb energy owing to the repulsion of the cations in the final state, but only atoms in the second coordination shell or beyond. The interpretation of feature I to originate from ICD with non-nearest neighbors is in line with the fact that it peaks toward 0 eV kinetic energy and only extends slightly above that, as well as with the observation of photons in coincidence with the three electrons, since the ground-state Kr^{2+} $4p^{-2}$ dication produced in the ICD process can afterward decay further by RCT (see Sec. IV B).

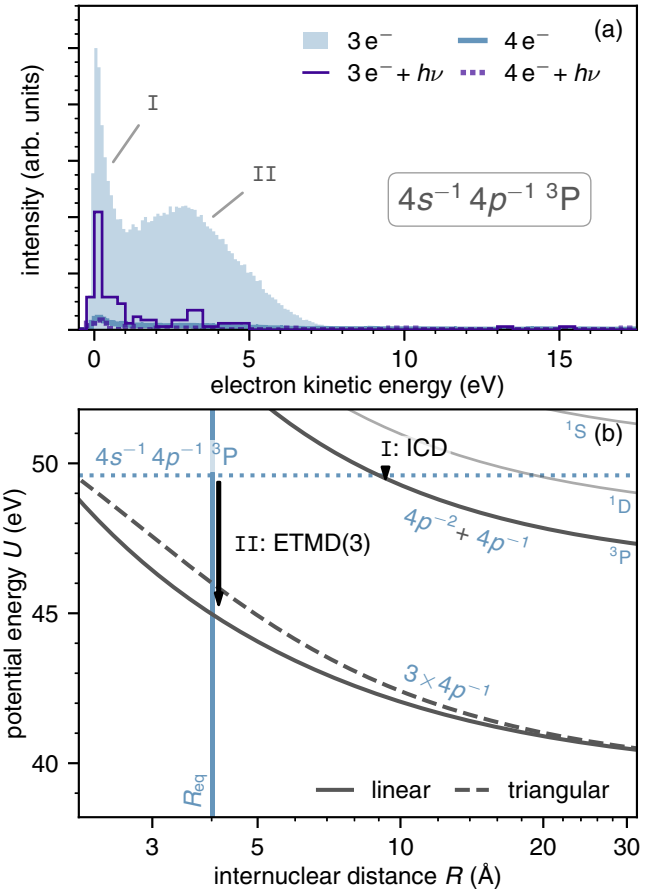


FIG. 5. Spectra of electrons (a) detected in the decay of the Kr^{2+} $4s^{-1}4p^{-1}$ ^3P state and potential energy curves (b) for final states of possible decay mechanisms relevant for this initial state. The spectra in panel (a) show the emission pattern, i.e., the kinetic energy of the (third and possibly fourth combined) electron(s) emitted after population of the Kr^{2+} state and the possible presence of a coincident photon in the decay cascade, for four different types of coincidence events that were detected. Here, two prominent features, labeled I and II, can be distinguished. Panel (b) shows an excerpt of Fig. 4 relevant for the considered initial state, where the features from panel (a) are attributed to certain transitions into the final-state PECs. See main text for a detailed discussion.

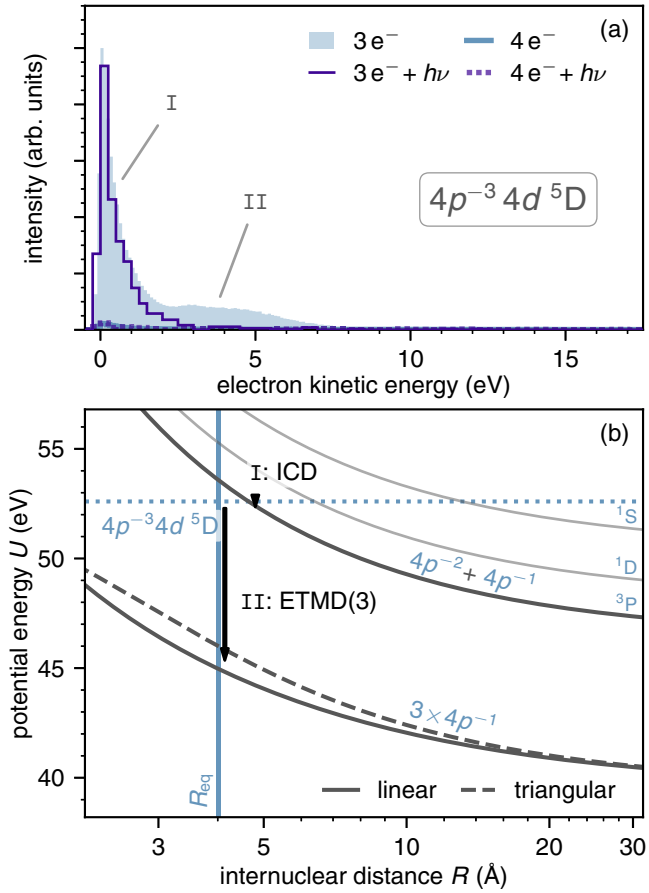


FIG. 6. Spectra of electrons (a) detected in correlation with the decay of the Kr^{2+} $4p^{-3}4d$ ^5D state and potential energy curves (b) for final states of possible decay mechanisms relevant for this initial state. The depiction is similar to that of Fig. 5. See main text for a detailed discussion.

The PEC diagram shows another final configuration that is accessible, namely, three singly ionized Kr^+ ground-state ions. From the $4s^{-1}4p^{-1}$ ^3P state, this configuration is reached via ETMD(3): A $4p$ electron from a neutral neighbor fills the $4s$ vacancy of the dication, thus making it a monocation, and a $4p$ electron from yet a different atom is emitted. Depending on the geometry of the three resulting ions, at R_{eq}, the ETMD(3) channel results in 3–4 eV kinetic energy of the electron, which is in good agreement with the experimental observation for feature II. The intensity ratio of these two specific ICD/ETMD variants should pose an interesting challenge for state-of-the-art theory.

D. Auger final state $4p^{-3}4d$ ^5D

With increasing binding energy, the next state with 18.2 eV excess energy with respect to the dicationic ground state is mainly of Kr^{2+} $4p^{-3}4d$ configuration. It mixes, however, with strong contributions from the $4s^{-1}4p^{-1}$ configuration [33]. The Kr^{2+} $4p^{-3}4d$ configuration corresponds to a ^5D term [28], while the $4s^{-1}4p^{-1}$ configuration couples to ^1P [33]. It should be noted that the atomic *LS*-coupling notation is not strictly valid for the relatively heavy Kr with atomic number $Z = 36$, and consequently, configuration mixing between different terms becomes possible and dipole selection rules are not strict. Nevertheless, both configurations need to be considered for the interpretation of the observed emission spectra, which are shown in Fig. 6 together with an enlarged view of the PEC diagram for the relevant final states. For simplicity, in the spectra and schemes we will refer to this state as Kr^{2+} $4p^{-3}4d$ ^5D according to the main contribution and literature assignments [28]. The accessible final states are the same as for the previously discussed $4s^{-1}4p^{-1}$ ^3P states; the difference is that the present initial states lie somewhat higher in energy (indicated by the dotted horizontal line). The emission spectrum of the third electron from $3\,e^-$ emission is similar to the $4s^{-1}4p^{-1}$ ^3P state composed of the two features I and II discernible in Fig. 6(a), which, however, now appear with changed intensity ratios. Feature I is observed in coincidence with photons, while no events with four

electrons (with or without photons) are detected. In general, both configurations can decay via ICD and ETMD(3). ICD from the $4p^{-3}4d$ ^{5}D initial states to either of the $4p^{-2}$ ^{3}P, ^{1}D, ^{1}S final states of the initial ion is dipole forbidden in *LS*-coupling notation; however, as mentioned, this restraint is not strictly prohibitive, but may lead to a higher contribution of the exchange component. For the ETMD(3) process starting from the Kr^{2+} $4p^{-3}4d$ configuration, a $4p$ electron is transferred from a neighboring atom to one of the three $4p$ vacancies, accompanied by a shakedown of the $4d$ electron also into the $4p$ orbital, whereby another neighbor is ionized, resulting overall in three Kr^+ $4p^{-1}$ ions.

The $4s^{-1}4p^{-1}$ ^{1}P configuration can decay by (dipole-allowed) ICD to the $4p^{-2}$ ^{1}D or ^{1}S states, or by (dipole-forbidden) ICD to the Kr^{2+} $4p^{-2}$ ^{3}P ground state. In Fig. 6(b), all possible final states are depicted. The ^{1}D or ^{1}S terms lie energetically higher by approximately 1.7 and 4.0 eV, respectively, compared to the Kr^{2+} $4p^{-2}$ ^{3}P ground state. Consequently, this ICD process will only be possible with partners at internuclear distances significantly larger than R_{eq}. It seems that ICD here has two options, either dipole-forbidden ICD with a partner close to R_{eq} or dipole-allowed ICD at significantly larger distances. Both scenarios may lead to an increased lifetime; thus, it is not surprising that ETMD(3) is again competitive. ETMD(3) from the Kr^{2+} $4s^{-1}4p^{-1}$ ^{1}P state will proceed as discussed in the previous subsection. From the present data, it cannot be disentangled how much of the spectrum results from a $4p^{-3}4d$ configuration of the initial state and how much from a $4s^{-1}4p^{-1}$ configuration. For Kr atoms, a ratio of about 1.85 favoring $4p^{-3}4d$ has been reported [33] but should not be straightforwardly adopted for clusters, as different shakeup probabilities have been observed there for Auger decays [36].

E. Auger final state $4p^{-3}4d$ ^{3}P

The next state also has a Kr^{2+} $4p^{-3}4d$ electron configuration, but with differing coupling resulting in a ^{3}P term. Its excess energy with respect to the dicationic ground state is 24.8 eV (59.2 eV total binding energy), i.e., significantly higher than the ^{5}D state considered in the previous subsection. The spectrum in Fig. 7(a) shows again two distinct features. Feature I peaks sharply at 0 eV and extends to about 2 eV, while feature II, which accounts for most of the spectrum's intensity, is rather broad and extends until 10 eV, with a maximum around 4 eV. Both features show up in the spectra where three electrons and one photon were detected in coincidence, but with slightly changed intensity compared to the three-electron case. For the first time, there is a significant intensity in the spectra of four emitted electrons, which is, however, concentrated at feature I. Feature II can be easily assigned with the help of the PEC diagram in Fig. 7(b). A direct ICD transition into the $Kr^{2+}(4p^{-2}$ ^{3}P$) + Kr^+(4p^{-1})$ delocalized final charge-state distribution is possible; here, only the ^{3}P component is relevant due to the spin selection rules and the ^{3}P nature of the initial state. At the equilibrium distance, about 5 eV excess energy is available for the ICD electron, which is slightly higher than the experimentally observed peak indicates. The contribution of ICD channels with neighbors at somewhat larger distances may explain the high-kinetic-energy tail. This interpretation agrees well with the observation of an additional photon, which is emitted in a subsequent RCT decay of the produced $Kr^{2+}(4p^{-2})$ dication. We used the fact that this feature is spectrally nicely isolated and always leads to emission of exactly three electrons and one photon for normalization of the relative intensities of the $3\,e^-$ and $3\,e^- + h\nu$ spectra in this and all other spectra using a scaling factor determined by the integral of the feature. ICD electrons from the Kr^{2+} $4p^{-3}4d$ state and the $Kr^{2+} + Kr^+$ breakup channel have been observed in dimers before [17], although with lower ICD electron kinetic energies because of the atomiclike energy levels of dimers.

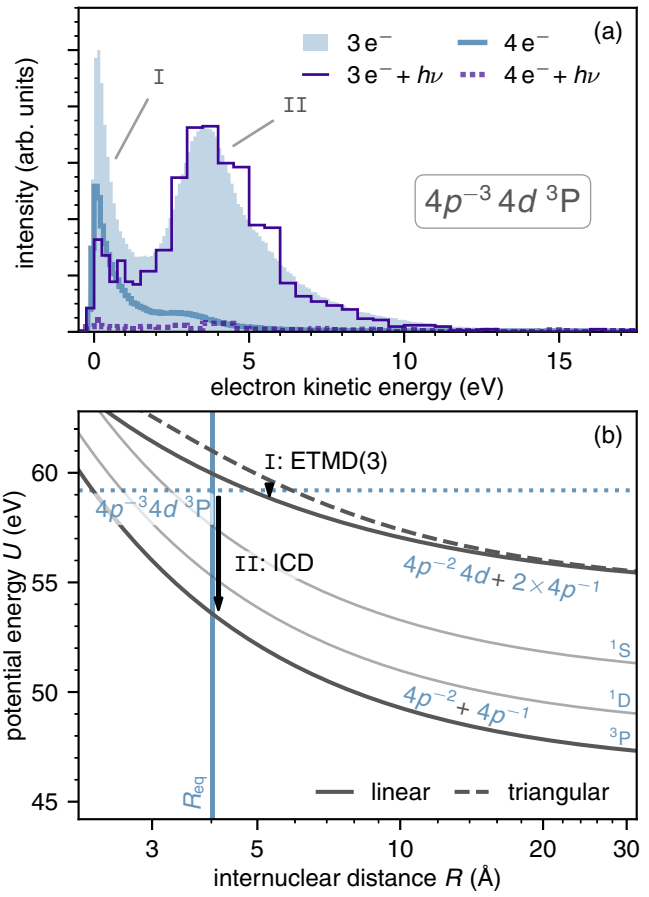


FIG. 7. Spectra of electrons (a) detected in correlation with the decay of the Kr^{2+} $4p^{-3}4d$ ^{3}P state and potential energy curves (b) for final states of possible decay mechanisms relevant for this initial state. The depiction is similar to that of Fig. 5. See main text for a detailed discussion.

Feature I has not been observed in dimers and its interpretation is more involved. We attribute feature I to ETMD(3). ETMD(3) cannot occur in dimers, but only in larger clusters, as three sites are necessary for it and, particularly, it cannot occur in dimers. As apparent from the coincidence spectra of Fig. 7(a), it corresponds to a competition of processes with emission of either four electrons *or* three electrons and one photon. The four-electron case is discussed first. The PEC diagram [Fig. 7(b)] shows that an ETMD(3) channel is open, in which one of the $4p$ vacancies of the excited ion is neutralized by an electron from a neutral neighbor and a third

Kr atom becomes ionized. The $4d$ electron does not participate in this decay. Following the common nomenclature of local autoionization processes, this process can be accordingly termed "spectator ETMD." In agreement with the experimental observation, the PECs suggest that the channel just opens at distances slightly larger than the equilibrium distance and produces electrons close to 0 eV kinetic energy. The final configuration of the excited ion in this case is Kr^+ $4p^{-2}4d$. Its binding energy cannot be deduced from the present spectra but can be estimated from the literature values for the atomic case to be approximately 15 eV above the Kr^+ ground state [30,37]. With a minimum electron binding energy for Kr clusters of about 12 eV, this excess energy is just sufficient for an ICD process with an atom directly neighboring it, producing another electron close to 0 eV (if Coulomb interaction with the other ions produced by ETMD is neglected). This cascade of an ETMD(3) and subsequent ICD process produces four electrons in total (together with the initial photoelectron and the Auger electron), two of which possess very low kinetic energies close to 0 eV.

Let us now discuss the case where instead of the fourth electron a UV photon is observed. Because the pathway above produces three singly charged ground-state ions, this photon cannot originate from a cascade ending with an RCT process. Instead, it is realistic that the ICD following ETMD proceeds with reduced efficiency. The presence of three Kr^+ ions, resulting from the preceding ETMD(3), will decrease the ICD efficiency for two reasons. First, additional Coulomb energy through interaction with these ions must be considered. Second, the cluster may start to disintegrate due to the Coulomb repulsion within the ICD lifetime, eventually producing a free ion with no neighbors available for ICD. The excited Kr^+ $4p^{-2}4d$ state may thus decay locally by a radiative transition emitting at least one photon in the UV range. For atoms, fluorescence transitions of this type have been observed in the VUV range [30].

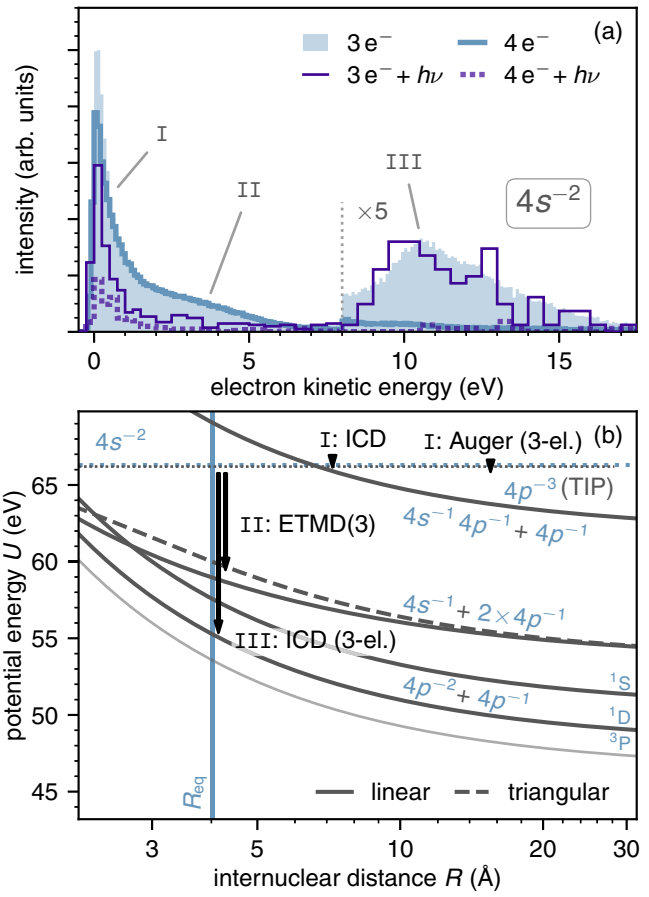


FIG. 8. Spectra of electrons (a) detected in correlation with the decay of the Kr^{2+} $4s^{-2}4p^6$ state and potential energy curves (b) for final states of possible decay mechanisms relevant for this initial state. The depiction is similar to that of Fig. 5. See main text for a detailed discussion.

F. Auger final state $4s^{-2}4p^6$

The state with highest binding energy that cannot undergo a second local Auger step (in atoms) is of Kr^{2+} $4s^{-2}4p^6$ electron configuration, i.e., with an empty $4s$ inner-valence subshell. Its excess energy with respect to the dicationic ground state was determined to 31.9 eV, which is about twice that of the Kr^{2+} $4s^{-1}4p^{-1}$ ^{3}P state. The emission spectra and the PEC diagram are shown in Fig. 8. Three features contribute: Feature I peaks sharply at 0 eV and extends to about 2 eV; it is observed in all spectra, i.e., in the emission of three and four electrons both with and without photons. Feature II appears as a shoulder to feature I, not showing a pronounced maximum but with a slowly decreasing intensity until about 6 eV. It is present in the emission spectra of three and four electrons, but no photon is detected in coincidence. The third feature (III) is weak, but has a clear maximum at about 10.5 eV kinetic energies. For better visibility, the scale is magnified by a factor of 5 above 8 eV in Fig. 8(a). Feature III apparently corresponds to a $3\,e^- + h\nu$ process, since it appears in the spectra of three electrons with and without photons, but not in those with four electrons.

From the PEC in Fig. 8(b), it can be deduced that the Kr^{2+} $4s^{-2}4p^6$ state can undergo ICD with a $4p$ electron filling one of the $4s$ vacancies, resulting in the Kr^{2+} $4s^{-1}4p^{-1}$ ^{3}P state and producing a neighboring Kr^+ ground-state ion. This channel is open at distances about twice as large as R_{eq}, resulting in the emission of an electron close to 0 eV and contributing to feature I. Through the population of the Kr^{2+} $4s^{-1}4p^{-1}$ ^{3}P state, the decay will proceed from there on as discussed in Sec. IV C. This means that another ICD step, followed by further charge delocalization via RCT or ETMD(3), is possible. The former explains the observation of $4\,e^- + h\nu$ coincidence events, while the latter contributes to feature II [see the spectra in Fig. 5(a)].

Alternatively, the Kr^{2+} $4s^{-2}4p^6$ state may relax by ETMD(3), with an electron filling one of the $4s$ vacancies and producing Kr^+ $4s^{-1}4p^6$ ions. The PEC diagram shows an excess energy of about 6 eV for the ETMD electron, and thus ETMD(3) may contribute to the high-energy tail of feature II. The resulting Kr^+ $4s^{-1}4p^6$ $^2S_{1/2}$ state still has a binding energy of about 26 eV [27]. It may further decay by ICD into two singly charged ground-state ions, but only at distances significantly larger than R_{eq}, or by a second ETMD(3) step. ETMD(3) may indeed be favored due to a considerably

lower Coulomb energy for suitable geometries. Both ICD and ETMD(3) would contribute to feature I and in total result in a $4\,e^-$ cascade (without photon emission). Since no photon is emitted in any scenario explaining feature II, this feature was used to normalize the intensity of four-electron emission to match the intensity of three-electron emission throughout the whole dataset.

Another pathway may contribute to feature I, which was not accessible for all previous states. As mentioned earlier, it is well established that the binding energies of ionic states are significantly reduced in clusters compared to atoms [38] due to polarization screening, with an increasing shift for higher charged states. For the Kr^{3+} tricationic ground state, shifts distributed around a value of about 8 eV have recently been reported [15], resulting in binding energies of around 66.2 eV (compared to 74.2 eV in atoms [28]). This range of values strongly overlaps with the range of binding energies of the Kr^{2+} $4s^{-2}4p^6$ state (see Table I) in clusters. The energetic shift due to polarization screening therefore opens a local Auger decay channel. Since the energies of the initial and final states are close, the Auger electron will possess only a low kinetic energy close to 0 eV. In general, the local Auger decay would be expected to dominate over any nonlocal channel. However, this particular Auger decay involves three electrons: two $4p$ electrons simultaneously filling both $4s$ holes and another $4p$ electron being ejected. This is a highly correlative process, sometimes termed TEOE (two-electron–one-electron), which has been observed before, but with a relatively weak intensity [39–41]. The resulting Kr^{3+} ground-state ion will decay further by ETMD(4), an ETMD variant that involves four atomic sites that has recently been observed [15]. Consequently, the Auger channel would also match the experimental observation of a four-electron coincidence without photon detection. From the present data, it cannot be disentangled how much these individual possible channels contribute to the total intensities of features I and II.

Finally, the weak but significant feature III shows the highest kinetic energy of all interatomic features observed in the present study, peaking around 10.5 eV. From the PEC diagram, it becomes clear that such a high kinetic energy can only be released in a three-electron ICD process. Here, both $4s$ vacancies are filled simultaneously by two $4p$ electrons of the same ion, and the excess energy is transferred to a neutral neighbor, thereby ionizing it. The populated $4p^{-2}$ final state is more likely to be the ^{1}D or ^{1}S state due to the singlet character of the $4s^{-2}$ ^{1}S initial state. Such correlative TEOE-ICD mechanisms have been observed in atomic dimers before [17,42]. This seemed, however, only possible due to the absence of additional sites and non-nearest neighbors for ETMD(3) or ICD at larger distances, respectively. The atomiclike electron binding energies in dimers furthermore do not facilitate the discussed newly opened Auger channel, leaving the TEOE-ICD as the only accessible electronic decay in dimers.

G. Double Auger decay

For Auger electron kinetic energies below approximately 20 eV, the Auger final-state binding energy of $\gtrsim$70 eV is large enough for further autoionization by a second Auger step in atoms, producing Kr^{3+} trications [28,29]. Auger cascades of two consecutive steps appear as islands of high intensity in the electron-electron correlation map of both emitted Auger electrons. The same final state can also be reached via direct double Auger decay, in which both electrons are emitted simultaneously. Here, the excess energy is shared among them, where a pair of one relatively fast and one relatively slow electron is favored. Direct double Auger decay manifests as diagonal lines of constant sum energy in the correlation map. For the decay of $3d^{-1}$ vacancies in Kr atoms, it was found that both direct and cascade double Auger decay contribute, with cascade Auger decay being dominant [28], similar to the cases of double autoionization decays of the Kr $3d^{-1}\,np$ resonances [43]. It is tempting to assume that a similar decay pattern can be observed for Kr clusters just with energetic shifts of the Auger final states, which is surprisingly not the case.

The energy range of interest is covered in the electron-electron correlation map shown in Fig. 2. It is strongly dominated by diagonal lines with high-intensity islands for different atomic Kr^{3+} states originating from the uncondensed atoms in the target jet. The atomic origin can be easily confirmed by the excellent agreement with literature values for the diagonal and island feature positions [28]. Besides a monotonically increasing intensity toward lower kinetic energies, no distinct features other than the atomic ones are discernible. A possible explanation for this observation is that, due to the reduced ionization potential in clusters and the availability of nonlocal channels, the number of emitted particles in this energy range is generally higher than 3. This is supported by the discussion in Sec. IV F, in which a significant emission of four and five particles was already observed. It is, therefore, instructive to investigate the emission of four ($4\,e^-$) or five ($4\,e^- + h\nu$) particles and to correlate them with the final-state energy of the first Auger step. The respective correlation maps are presented in Figs. 9 ($4\,e^-$) and 10 ($4\,e^- + h\nu$). Here, both the third and the fourth detected electrons are considered for the correlation map. The solid line in panel (b) represents the respective projection onto the Auger final-state axis. For comparison, the projection from the three-electron map [Fig. 2(b)] is also shown as a shaded area in Fig. 9, and the projection from Fig. 9 is included in Fig. 10. Panel (c) shows the projection on the energy axis of the third and fourth electron combined (solid line), as well as the projection of only the third electron (dashed line).

The appearance of states with Auger final-state energy below ~70 eV (kinetic energies higher than 20 eV) has already been discussed in detail. In the presentation of four- and five-particle coincidences, one more Auger final state becomes distinguishable at 74.8 eV binding energy (40.2 eV excess energy compared to the dicationic ground state; see Table I). The assignment of this state is not as straightforward as in the previous cases. In the atomic spectrum, two states are energetically close and could contribute, namely, those of $4s^{-1}4p^{-2}\,5s$ and $4p^{-4}4d^2$ configurations. For simplicity, we will use the former for labeling the state in the figures. Due to the accessibility of both local and nonlocal decay channels, the possible decay pathways become more complex now, but a discussion can nevertheless be attempted with the help of the emission spectra and corresponding region of interest in the

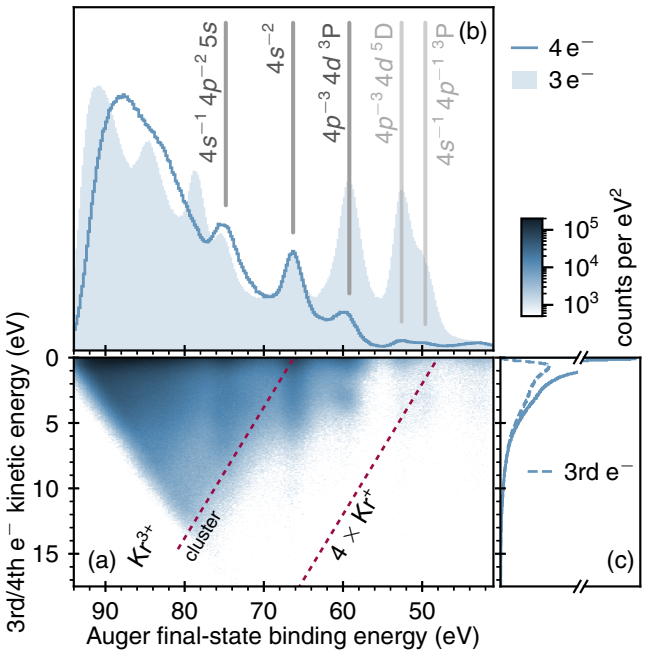


FIG. 9. Coincidence map similar to that shown in Fig. 2, representing correlations between electrons leading to the population of the Kr^{2+} Auger final states [panel (b)] and a subsequently emitted third electron [panel (c)]. Here, only those events where exactly four electrons have been detected in coincidence are shown in the map [panel (a)] and as solid lines in panels (b) and (c), with the three-electron spectrum from Fig. 2 depicted as a shaded area in panel (b) for reference with one fewer electron.

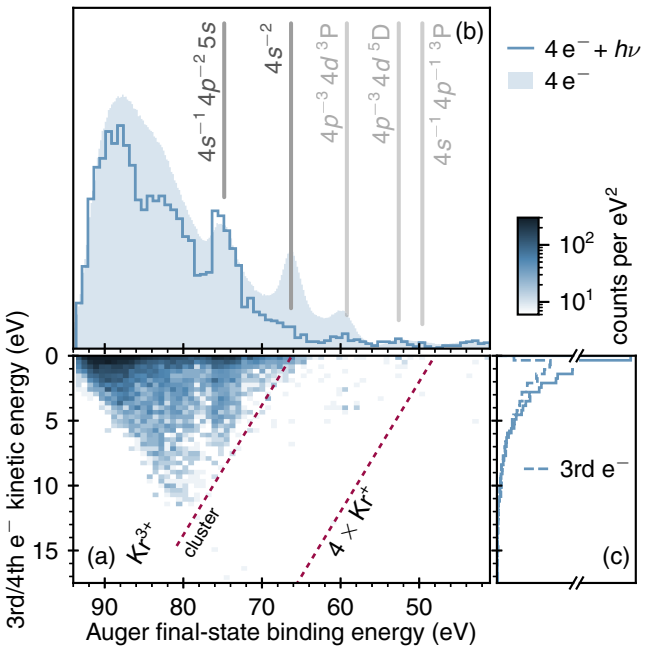


FIG. 10. Coincidence map similar to that shown in Fig. 2, representing correlations between electrons leading to the population of the Kr^{2+} Auger final states [panel (b)] and subsequently emitted third and fourth electron [panel (c)]. Here, only those events where exactly four electrons and an additional UV photon have been detected in coincidence are shown in the map [panel (a)] and as solid lines in panels (b) and (c), with the four-electron spectrum from Fig. 9 depicted as a shaded area in panel (b) for reference without a photon.

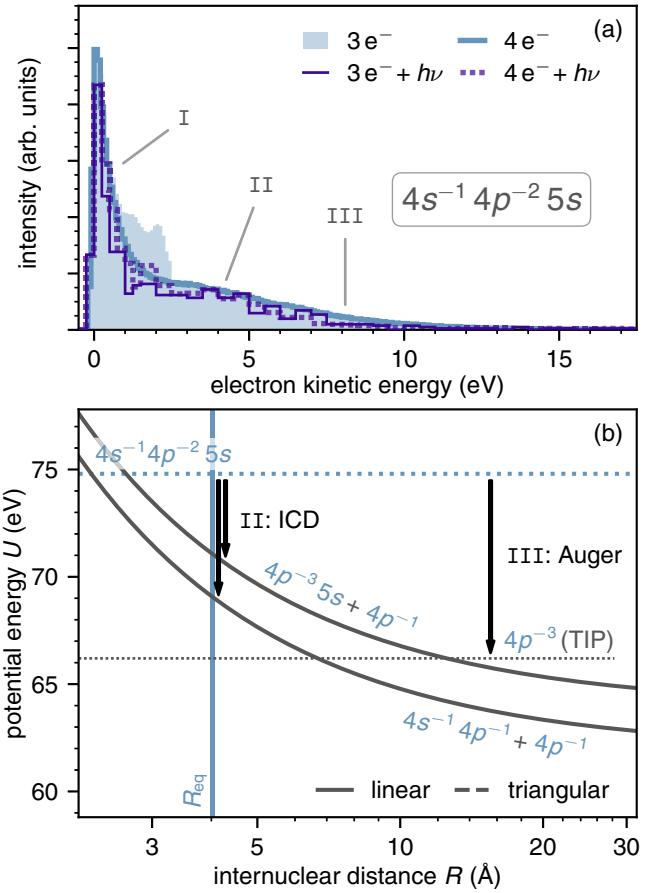


FIG. 11. Spectra of electrons (a) detected in correlation with the decay of the Kr^{2+} $4s^{-1}4p^{-2}\,5s$ state and potential energy curves (b) for final states of possible decay mechanisms relevant for this initial state. The depiction is similar to that of Fig. 5. See main text for a detailed discussion.

PEC diagram shown in Fig. 11. From the total binding energy of this feature and the triple-ionization potential in clusters, it can be estimated that local Auger electrons should be emitted with about 8.6 eV kinetic energy. However, the observation that this spectral range exhibits only weak intensity suggests that Auger decay to the tricationic ground state plays only a minor role. Instead, the characteristic peak at 0 eV with a pronounced shoulder at kinetic energies of a few eV supports the occurrence of interatomic processes, likely as a cascade with some of the previously discussed configurations as intermediate states.

The dominance of interatomic channels over local Auger decay may seem surprising. However, it can be understood in terms of an ioniclike character of excited cluster states with a high principal quantum number n [36]. In this case, much of the Rydberg electron's wavefunction is highly delocalized over several coordination shells [44], in such a way that the excited dication may actually behave like a trication. It is a remarkable observation that there is no clear cluster analog to the atomic double Auger decay features discernible in any of the correlation maps; only a structureless increasing emission intensity for slow electrons is observed for higher Auger final-state energies. In atomic Kr, the states undergoing double

Auger decay are highly excited with one or two electrons in Rydberg-like orbitals. As argued above, the character of such states may be strongly influenced by wavefunction amplitude at the positions of the neighboring atoms up to an extent that these states do not even exist in terms of atomic state notation.

V. CONCLUSION

In this article, we provide an extensive study of the decay of the $3d^{-1}$ vacancy in Kr clusters using a multicoincidence technique with up to four electrons and a UV photon detected from the relaxation cascade. The first step of the cascade is dominated by Auger decay, which efficiently populates excited Kr^{2+} states. We consider the six most intensely populated Auger final states and discuss them individually in detail.

The coincidence method enables a comprehensive study of each individual state, accompanied by estimates of potential energy curves for possible final states of interatomic decay processes (see Fig. 4). Although these states—with one exception—are known to relax purely radiatively in atoms, we show that in clusters, a large variety of interatomic processes leads to the emission of additional electrons and/or photons in the decay cascade of *all* Auger final states.

The rich relaxation cascade of the Kr $3d^{-1}$ vacancy is composed of variants of the ICD, ETMD(3), and RCT processes, including exotic kinds such as three-electron ICD. From observation of RCT following ICD, we can conclude that the cluster typically fragments into larger pieces instead of isolated ions, enabling further nonlocal decay. Throughout the study, it became clear that interatomic processes complete the relaxation cascade in every case, resulting in charge distribution within the cluster and its eventual fragmentation. More precisely, due to the larger number of available final states for increasing binding energies of the populated Auger final states, the decay cascade becomes more complex as the Auger electron energy decreases. As a result, the average number of ejected particles increases from 1 (only a photon in the case of the ionic ground state) to 3 for the highest excited Auger final state considered, where, for example, two consecutive ICD processes lead to a concluding RCT process.

ACKNOWLEDGMENTS

We would like to thank Lorenz Cederbaum and Alexander Kuleff for stimulating discussions. We acknowledge Synchrotron SOLEIL for provision of beamtime and we would like to thank the staff for assistance in using the PLEIADES beamline under Proposal No. 20210883. We thank the Helmholtz-Zentrum Berlin für Materialien und Energie (HZB) for the allocation of synchrotron radiation beamtime at the UE56-2_PGM-2 beamline at the BESSY II storage ring (Proposal No. Photons-192-08804-ST). This work was supported by the German Federal Ministry of Education and Research (BMBF) with the projects 05K22RK2—GPhaseCC, 05K22RK1—TRANSALP, and 05K25RK2—iXCOVER as well as SFB 1319 ELCH, funded by the Deutsche Forschungsgemeinschaft (German Research Foundation, DFG; Project No. 328961117). F.T. also acknowledges funding by the DFG—Project No. 509471550, Emmy Noether Programme.

DATA AVAILABILITY

The data that support the findings of this article are not publicly available upon publication because it is not technically feasible and/or the cost of preparing, depositing, and hosting the data would be prohibitive within the terms of this research project. The data are available from the authors upon reasonable request.

[1] V. Jonauskas, L. Partanen, S. Kučas, R. Karazija, M. Huttula, S. Aksela, and H. Aksela, Auger cascade satellites following 3d ionization in xenon, J. Phys. B: At. Mol. Opt. Phys. **36**, 4403 (2003).

[2] F. Penent, P. Lablanquie, R. I. Hall, J. Palaudoux, K. Ito, Y. Hikosaka, T. Aoto, and J. H. D. Eland, Coincidence Auger spectroscopy, J. Electron Spectrosc. Relat. Phenom. **144–147**, 7 (2005).

[3] Y. Hikosaka, P. Lablanquie, F. Penent, T. Kaneyasu, E. Shigemasa, J. H. D. Eland, T. Aoto, and K. Ito, Single, double, and triple Auger decay of the Xe 4*p* core-hole states, Phys. Rev. A **76**, 032708 (2007).

[4] P. Lablanquie, M. A. Khalal, L. Andric, J. Palaudoux, F. Penent, J.-M. Bizau, D. Cubaynes, K. Jänkälä, Y. Hikosaka, K. Ito, K. Bučar, and M. Žitnik, Multi-electron coincidence spectroscopy: Triple Auger decay of Ar 2p and 2s holes, J. Electron Spectrosc. Relat. Phenom. **220**, 125 (2017).

[5] R. Guillemin, K. Jänkälä, B. Cunha de Miranda, T. Marin, L. Journel, T. Marchenko, O. Travnikova, G. Goldsztejn, I. Ismail, R. Püttner, D. Céolin, B. Lassalle-Kaiser, M. N. Piancastelli, and M. Simon, Interplay of complex decay processes after argon 1*s* ionization, Phys. Rev. A **97**, 013418 (2018).

[6] T. Jahnke, U. Hergenhahn, B. Winter, R. Dörner, U. Frühling, P. V. Demekhin, K. Gokhberg, L. S. Cederbaum, A. Ehresmann, A. Knie, and A. Dreuw, Interatomic and intermolecular Coulombic decay, Chem. Rev. **120**, 11295 (2020).

[7] L. S. Cederbaum, J. Zobeley, and F. Tarantelli, Giant intermolecular decay and fragmentation of clusters, Phys. Rev. Lett. **79**, 4778 (1997).

[8] S. Marburger, O. Kugeler, U. Hergenhahn, and T. Möller, Experimental evidence for interatomic Coulombic decay in Ne clusters, Phys. Rev. Lett. **90**, 203401 (2003).

[9] V. Averbukh, I. B. Müller, and L. S. Cederbaum, Mechanism of interatomic Coulombic decay in clusters, Phys. Rev. Lett. **93**, 263002 (2004).

[10] T. Jahnke, A. Czasch, M. Schöffler, S. Schössler, M. Käsz, J. Titze, K. Kreidi, R. E. Grisenti, A. Staudte, O. Jagutzki, L. P. H. Schmidt, T. Weber, H. Schmidt-Böcking, K. Ueda, and R. Dörner, Experimental separation of virtual photon exchange and electron transfer in interatomic Coulombic decay of neon dimers, Phys. Rev. Lett. **99**, 153401 (2007).

[11] A. Kivimäki, S. L. Sorensen, M. Tchaplyguine, M. Gisselbrecht, R. R. T. Marinho, R. Feifel, G. Öhrwall, S. Svensson, and O. Björneholm, Resonant Auger spectroscopy

of argon clusters at the $2p$ threshold, Phys. Rev. A **71**, 033204 (2005).

[12] R. Santra, J. Zobeley, and L. S. Cederbaum, Electronic decay of valence holes in clusters and condensed matter, Phys. Rev. B **64**, 245104 (2001).

[13] K. Sakai, S. Stoychev, T. Ouchi, I. Higuchi, M. Schöffler, T. Mazza, H. Fukuzawa, K. Nagaya, M. Yao, Y. Tamenori, A. I. Kuleff, N. Saito, and K. Ueda, Electron-transfer-mediated decay and interatomic Coulombic decay from the triply ionized states in argon dimers, Phys. Rev. Lett. **106**, 033401 (2011).

[14] M. Förstel, M. Mucke, T. Arion, A. M. Bradshaw, and U. Hergenhahn, Autoionization mediated by electron transfer, Phys. Rev. Lett. **106**, 033402 (2011).

[15] L. Marder, C. Küstner-Wetekam, N. Kiefer, J. Viehmann, N. Golchert, E. Heikura, F. Trinter, D. Cubaynes, J. Palaudoux, F. Penent, A. Ehresmann, L. S. Cederbaum, P. Kolorenč, and A. Hans, Neutralization of multiply charged ground-state ions by collective electron transfer from an environment, Phys. Rev. Lett. **135**, 053201 (2025).

[16] N. Saito, Y. Morishita, I. H. Suzuki, S. D. Stoychev, A. I. Kuleff, L. S. Cederbaum, X.-J. Liu, H. Fukuzawa, G. Prümper, and K. Ueda, Evidence of radiative charge transfer in argon dimers, Chem. Phys. Lett. **441**, 16 (2007).

[17] K. Ueda, H. Fukuzawa, X.-J. Liu, K. Sakai, G. Prümper, Y. Morishita, N. Saito, I. Suzuki, K. Nagaya, H. Iwayama, M. Yao, K. Kreidi, M. Schöffler, T. Jahnke, S. Schössler, R. Dörner, T. Weber, J. Harries, and Y. Tamenori, Interatomic Coulombic decay following the Auger decay: Experimental evidence in rare-gas dimers, J. Electron Spectrosc. Relat. Phenom. **166–167**, 3 (2008).

[18] M. R. Weiss, R. Follath, K. J. S. Sawhney, F. Senf, J. Bahrdt, W. Frentrup, A. Gaupp, S. Sasaki, M. Scheer, H.-C. Mertins, D. Abramsohn, F. Schäfers, W. Kuch, and W. Mahler, The elliptically polarized undulator beamlines at BESSY II, Nucl. Instrum. Methods Phys. Res. Sect. A **467–468**, 449 (2001).

[19] T. Arion, M. Mucke, M. Förstel, A. M. Bradshaw, and U. Hergenhahn, Interatomic Coulombic decay in mixed NeKr clusters, J. Chem. Phys. **134**, 074306 (2011).

[20] M. Mucke, M. Förstel, T. Lischke, T. Arion, A. M. Bradshaw, and U. Hergenhahn, Performance of a short "magnetic bottle" electron spectrometer, Rev. Sci. Instrum. **83**, 063106 (2012).

[21] A. Hans, C. Ozga, P. Schmidt, G. Hartmann, A. Nehls, P. Wenzel, C. Richter, C. Lant, X. Holzapfel, J. H. Viehmann, U. Hergenhahn, A. Ehresmann, and A. Knie, Setup for multicoincidence experiments of photons in the extreme ultraviolet to visible spectral range and charged particles—The solid angle maximization approach, Rev. Sci. Instrum. **90**, 093104 (2019).

[22] A. Hans, C. Küstner-Wetekam, P. Schmidt, C. Ozga, X. Holzapfel, H. Otto, C. Zindel, C. Richter, L. S. Cederbaum, A. Ehresmann, U. Hergenhahn, N. V. Kryzhevoi, and A. Knie, Core-level interatomic Coulombic decay in van der Waals clusters, Phys. Rev. Res. **2**, 012022(R) (2020).

[23] A. Hans, P. Schmidt, C. Ozga, G. Hartmann, X. Holzapfel, A. Ehresmann, and A. Knie, Extreme ultraviolet to visible dispersed single photon detection for highly sensitive sensing of fundamental processes in diverse samples, Materials **11**, 869 (2018).

[24] J. H. D. Eland, O. Vieuxmaire, T. Kinugawa, P. Lablanquie, R. I. Hall, and F. Penent, Complete two-electron spectra in double photoionization: The rare gases Ar, Kr, and Xe, Phys. Rev. Lett. **90**, 053003 (2003).

[25] U. Buck and R. Krohne, Cluster size determination from diffractive He atom scattering, J. Chem. Phys. **105**, 5408 (1996).

[26] O. F. Hagena and W. Obert, Cluster formation in expanding supersonic jets: Effect of pressure, temperature, nozzle size, and test gas, J. Chem. Phys. **56**, 1793 (1972).

[27] R. Feifel, M. Tchaplyguine, G. Öhrwall, M. Salonen, M. Lundwall, R. R. T. Marinho, M. Gisselbrecht, S. L. Sorensen, A. Naves de Brito, L. Karlsson, N. Mårtensson, S. Svensson, and O. Björneholm, From localised to delocalised electronic states in free Ar, Kr and Xe clusters, Eur. Phys. J. D **30**, 343 (2004).

[28] J. Palaudoux, P. Lablanquie, L. Andric, K. Ito, E. Shigemasa, J. H. D. Eland, V. Jonauskas, S. Kučas, R. Karazija, and F. Penent, Multielectron spectroscopy: Auger decays of the krypton $3d$ hole, Phys. Rev. A **82**, 043419 (2010).

[29] E. Andersson, S. Fritzsche, P. Linusson, L. Hedin, J. H. D. Eland, J.-E. Rubensson, L. Karlsson, and R. Feifel, Multielectron coincidence study of the double Auger decay of $3d$-ionized krypton, Phys. Rev. A **82**, 043418 (2010).

[30] M. Wildberger, A. Ehresmann, H. Schmoranzer, B. Möbus, B. Magel, and K.-H. Schartner, Fluorescence studies on the 3d-ionization threshold range in krypton, Phys. Lett. A **193**, 274 (1994).

[31] O. Björneholm, F. Federmann, F. Fössing, T. Möller, and P. Stampfli, Core level binding energy shifts and polarization screening: A combined experimental and theoretical study of argon clusters, J. Chem. Phys. **104**, 1846 (1996).

[32] G. Öhrwall, R. F. Fink, M. Tchaplyguine, L. Ojamäe, M. Lundwall, R. R. T. Marinho, A. Naves de Brito, S. L. Sorensen, M. Gisselbrecht, R. Feifel, T. Rander, A. Lindblad, J. Schulz, L. J. Sæthre, N. Mårtensson, S. Svensson, and O. Björneholm, The electronic structure of free water clusters probed by Auger electron spectroscopy, J. Chem. Phys. **123**, 054310 (2005).

[33] J. Jauhiainen, H. Aksela, S. Aksela, A. Kivimaki, O. P. Sairanen, E. Nommiste, and J. Vegh, Correlation satellites in the Xe $N_{4,5}$-OO and Kr $M_{4,5}$-NN Auger spectra, J. Phys. B: At. Mol. Opt. Phys. **28**, 3831 (1995).

[34] X. Sheng, J. P. Toennies, and K. T. Tang, Conformal analytical potential for all the rare gas dimers over the full range of internuclear distances, Phys. Rev. Lett. **125**, 253402 (2020).

[35] C. Küstner-Wetekam, L. Marder, D. Bloß, C. Honisch, N. Kiefer, C. Richter, S. Rubik, R. Schaf, C. Zindel, M. Förstel, K. Gokhberg, A. Knie, U. Hergenhahn, A. Ehresmann, P. Kolorenč, and A. Hans, Experimental quantification of site-specific efficiency of interatomic Coulombic decay after inner shell ionization, Commun. Phys. **6**, 50 (2023).

[36] S. Peredkov, A. Kivimäki, S. L. Sorensen, J. Schulz, N. Mårtensson, G. Öhrwall, M. Lundwall, T. Rander, A. Lindblad, H. Bergersen, S. Svensson, O. Björneholm, and M. Tchaplyguine, Ioniclike energy structure of neutral core-excited states in free Kr clusters, Phys. Rev. A **72**, 021201(R) (2005).

[37] E. B. Saloman, Energy levels and observed spectral lines of krypton, Kr I through Kr XXXVI, J. Phys. Chem. Ref. Data **36**, 215 (2007).

[38] M. Lundwall, R. F. Fink, M. Tchaplyguine, A. Lindblad, G. Öhrwall, H. Bergersen, S. Peredkov, T. Rander, S. Svensson, and O. Björneholm, Shell-dependent core-level chemical shifts

observed in free xenon clusters, J. Phys. B: At. Mol. Opt. Phys. **39**, 5225 (2006).

[39] J. H. D. Eland, R. J. Squibb, M. Mucke, S. Zagorodskikh, P. Linusson, and R. Feifel, Direct observation of three-electron collective decay in a resonant Auger process, New J. Phys. **17**, 122001 (2015).

[40] M. Mailhiot, K. Jänkälä, M. Huttula, M. Patanen, K. Bučar, M. Žitnik, D. Cubaynes, F. Holzmeier, R. Feifel, D. Céolin, L. Andric, R. Guillemin, I. Ismail, J. Palaudoux, F. Penent, and P. Lablanquie, Multielectron coincidence spectroscopy of the $Ar^{2+}(2p^{-2})$ double-core-hole decay, Phys. Rev. A **107**, 063108 (2023).

[41] M. Žitnik, R. Püttner, G. Goldsztejn, K. Bučar, M. Kavčič, A. Mihelič, T. Marchenko, R. Guillemin, L. Journel, O. Travnikova, D. Céolin, M. N. Piancastelli, and M. Simon, Two-to-one Auger decay of a double L vacancy in argon, Phys. Rev. A **93**, 021401(R) (2016).

[42] T. Ouchi, K. Sakai, H. Fukuzawa, X.-J. Liu, I. Higuchi, Y. Tamenori, K. Nagaya, H. Iwayama, M. Yao, D. Zhang, D. Ding, A. I. Kuleff, S. D. Stoychev, P. V. Demekhin, N. Saito, and K. Ueda, Three-electron interatomic Coulombic decay from the inner-valence double-vacancy states in NeAr, Phys. Rev. Lett. **107**, 053401 (2011).

[43] M. Y. Amusia, V. A. Kilin, A. Ehresmann, H. Schmoranzer, and K. H. Schartner, Double-autoionization decay of resonantly excited single-electron states, J. Phys. B: At. Mol. Opt. Phys. **26**, 1281 (1993).

[44] J. P. Gauyacq, Core-excited $Ar^*(2p_{3/2}^{-1}\,nl)$ atoms inside an Ar crystal: Effect of Ar neighbors on the excited state, Phys. Rev. B **71**, 115433 (2005).